Flow rate variations in microfluidic circuits with free surfaces

Taha Messelmani, Isabela Zarpellon Nascimento, Eric Leclerc, Cécile
Legallais, Adam Meziane, William César, Rachid Jellali, Anne Le Goff

Flow rate variations in microfluidic circuits with free surfaces

Taha Messelmani
University of Technology of Compiègne

Isabela Zarpellon Nascimento
University of Technology of Compiègne

Eric Leclerc
Laboratory for Integrated Micro-Mechatronic Systems

Cécile Legallais
University of Technology of Compiègne

Adam Meziane
Fluigent (France)

William César
Fluigent (France)

Rachid Jellali
University of Technology of Compiègne

Anne Le Goff (✉ anne.le-goff@utc.fr)
University of Technology of Compiègne

Flow rate variations in microfluidic circuits with free surfaces

Taha Messelmani[1†], Isabela Zarpellon Nascimento[1†], Eric Leclerc[1,2], Cécile Legallais[1], Adam Meziane[3], William César[3], Rachid Jellali[1] and Anne Le Goff[1*]

[1]Biomechanics and Bioengineering UMR 7338, Université de technologie de Compiègne, CNRS, Centre de Recherche Royallieu CS 60319, Compiègne, 60203 Cedex, France.
[2]IRL 2820 LIMMS, CNRS IIS Institute of Industrial Science, University of Tokyo, 4-6-1 Komaba, Meguro ku, Tokyo, 153-8505, Japan.
[3]Fluigent, 67 avenue de Fontainebleau, Le Kremlin-Bicêtre, 94 270, France.

*Corresponding author(s). E-mail(s): anne.le-goff@utc.fr;
[†]These authors contributed equally to this work.

Abstract

We investigate analytically and experimentally the flow rate through a biochip in a circuit involving a peristaltic pump and reservoirs with liquid/air interfaces. Peristaltic pumps are a convenient way to achieve recirculation in microfluidic circuits. We consider different cases: reservoirs in contact with ambient air, tight reservoirs, and imperfect tightness leading to air or liquid leaks. We demonstrate that if changes in hydraulic resistance are slow enough, i.e. if cells do not proliferate too fast, the system may reach an equilibrium, with a difference in liquid height between inlet and outlet reservoir compensating the pressure drop in the biochip. We compute the flow rate through the biochip in the transient regime as well as the characteristic time. We also show that depending on the circuit dimensions, this equilibrium may never be reached. We provide guidelines to design tubings and reservoirs to avoid this situation and ensure a smooth recirculation at a desired flow rate, which is a necessary condition for dynamic cell culture.

Keywords: microfluidic, pressure control, free surface, cell culture

1 Introduction

Different technologies exist to pump fluids through microfluidic cell culture chambers [1]. Passive pumping can be achieved [2] thanks to gravity [3], surface tension [4], or osmosis [5]. Placing the microfluidic circuit on a rotating disk allows to use centrifugal force as a driving force [6]. In many microfluidic cell culture systems however, medium is actively pumped through the culture chambers.

All types of pumps can either push the fluid through the inlet or suck it from the outlet [7]. Syringe pumps are commonly encoutered in microfluidics laboratories but flows driven by syringe pumps are subjected to fluctuations [8]. It has been shown that the type of flow control can influence the poly-dispersity of emulsions generated in microsystems [9]. Pressure control has been proposed as an alternative. The difference between flow-rate control using syringe or peristaltic pumps and pressure pumps has mostly been studied in the case of immiscible [10] or miscible [11] two-phase flows. Guidelines have been provided to adapt the design of channels to pressure flow control [12, 13]. Positive pressure at the inlet can be imposed by a pressure manifold fed with compressed air [14, 15] or by fluid columns [16].

For organ-on-chip applications, the fluid needs to be recirculated through the system to mimic the closed loop circulation of blood in the body [17]. Liquid recirculation in such microfluidic circuits is a challenge [18, 19] and requires pumps [1] and/or valves [20]. In this manuscript, we investigate the flow in a microfluidic biochip installed between an inlet and an outlet reservoir, in the presence of cells. The biochip accommodates cells that proliferate over time during the experiment, and require feeding and oxygenation with a culture medium. To achieve recirculation, a peristaltic pump drives the liquid from the outlet to the inlet reservoir. We study the influence of cell growth on the overall circuit resistance and compute the difference between the target flow rate Q imposed by the pump and the flow rate through the biochip Q' under different conditions: we consider a tight circuit, a leaking seal and a leaking connector.

2 Methods

2.1 Bioreactor design and operation

Dynamic cell culture is performed in PDMS biochips. Each chip has a volume of $40 \, \mu L$ and a surface of $2 \, cm^2$. Cells reside at the textured bottom while medium flows above them through the smooth top chamber. To operate in parallel with 12 biochips, we use an Integrated Dynamic Cell Cultures in Microsystems (IDCCM) tool box, previously developed in our team and illustrated in supplementary figure A1 [21]. Briefly, this platform, made of polycarbonate, consists of 3 parts: a 24-well plate equipped with connectors at the bottom of each reservoir that can be plugged into the biochips, a cover with connectors,

and a PDMS seal. Tightness is achieved by inserting the assembled platform in a metal frame maintained by a clamp whose strength can be adjusted.

2.2 Tightness assays

The test is conducted using the 24-well platform. Using silicon tubes and T-connectors, the outlet of the pressure controller is connected to the inlet of 12 wells as illustrated in figure 1(a). The pressurized wells are those of the rows placed at the edges of the platform. Their bottom outlets are sealed. This way, half of the wells are pressurized, mimicking what happens when the peristaltic pump is used to circulate the culture medium in the biochips. Wells that are not connected to the pressure controller can be either sealed or left open. The platform is then immersed in water in a glass container. The inlet pressure is increased by 20 mbar steps until visible bubbles indicate a leak. The test is performed twice with two degrees of fastening force. Two clamps on each side of the device squeeze the three layer between their jaws and tighten the wells. A threaded rod is used to adjust the tightening strength.
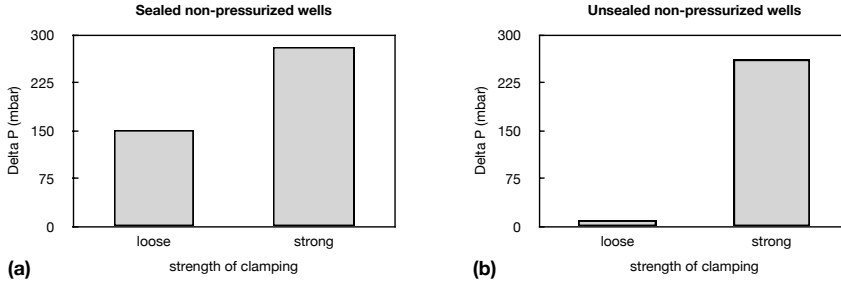
2.3 Cell culture

We use the hepatic cell line HepG2/C3A, a clone of the HepG2 line derived from human hepatocellular carcinoma (ATCC CRL-10741). Cells are cultured at $37°C$ and 5% CO_2 in a humid atmosphere in 75 cm^2 flasks. The culture medium is Minimal Essential Medium (MEM) with phenol red (Pan Biotech, Aidenbach, Germany) supplemented with 10% (v/v) fetal bovine serum (Gibco, Waltham, MA, USA), 2 mM L-glutamine (Gibco), 0.1 mM non-essential amino acids (Gibco), 1 mM sodium pyruvate (Gibco), and 100 U/mL penicillin/streptomycin (Pan Biotech). Cells are passaged weekly at a confluence of 80-90% and the culture medium is renewed every two days. Biochips coated with collagen (Corning, NY, USA) are seeded with the desired number of cells suspended in 80 μL of culture medium, kept 24 h in static conditions at $37°C$ and 5% CO_2. Then, a flow rate of 10μL/min is imposed by a peristaltic pump (ISM949, ISMATEC) using silicone tubing of 0.089 cm internal diameter (PharMed BTP, Cole Parmer). The process is illustrated in supplementary figure A1. The number of cells in a biochip is evaluated by injecting a known volume of a trypsin-EDTA solution (0.25%, Gibco) to detach the cells from the chip surface, and measure the final cell number using a Malassez slide. These measurements are performed 24 h after cell seeding to evaluate the adhesion rate and at different time points during microfluidic culture to evaluate the proliferation of adherent cells.

2.4 Flow control

For most experiments, flow is driven by a peristaltic pump (ISM949, ISMATEC) using silicone tubing of 0.089 cm internal diameter (PharMed BTP, Cole Parmer). The flow rate varies between 10 and 25 μL/min.

To evaluate the time evolution of hydraulic resistance in biochips during cell culture, the flow rate is imposed, instead of a peristaltic pump, by a pressure controller (MFCS-EX, Fluigent, Le Kremlin-Bicêtre, France), a flowmeter (Flow Unit type M, Fluigent) and a feedback loop. The pressure drop (pressure difference between inlet and outlet reservoirs) is evaluated for flow rates ranging from 0 to 30 μL/min.

2.5 Numerical calculation

Numerical integration of differential equations is performed in Python using scipy.integrate subpackage. A fifth-order implicit Runge-Kutta method is chosen in order to avoid non-physical oscillations.

3 Results

3.1 Tightness assay

Fig. 1 Experimental setup to assess tightness. (a) Configuration mimicking the perfusion of 12 biochips. (b) Configuration used to assess the tightness of a single well.

The dynamic culture system consists of a lid, a silicone seal and a 24-well plate. In cell culture experiments, biochips can be installed between two neighboring wells by plugging them to the connectors found at the bottom of each well. In a similar manner, liquid can be transferred from one well to another using a peristaltic pump and deformable tubing inserted in two of the 24 holes pierced in the lid. Lid, seal and well plate are aligned and assembled using a metal plate holder. For tightness assays, in order to mimic the conditions encountered in dynamic cell culture, we pressurized the wells of the two outer rows. Wells of the two central rows were closed with a plug. We used two positions of the threaded rod, respectively corresponding to a loose and tight clamping. For the loosest clamping, air leakage was observed at the silicone seal when the relative pressure in the wells reached 150 mbar, while for the strongest clamping, leakage at the seal only occurred for a pressure of 280 mbar. When the central wells were left open, leaks occurred at lower relative pressure: 10 mbar for the loose clamping and 260 mbar for the tight one. In tight clamping conditions, leakage was only observed at the central non-pressurized wells (positions B3 and B4, according to Figure 1(b)). In a second experiment, only one well was pressurized at a time, as illustrated in figure 1 (b). When the
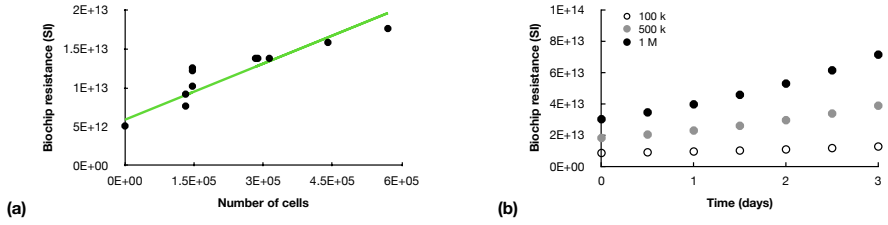
wells in positions A1 and A6 were pressurized, no leakage was observed (the pressure was increased up to 750 mbar). On the other hand, for the wells in positions A2 to A5, leakage at the seal occurred when the pressure reached 300 mbar. Each time, the bubbles formed at the same point of the seal, in the center of the edge, indicating that the sealing is less effective at this region.

Fig. 2 Tightness assessment in the configuration mimicking the perfusion of 12 biochips, with non-pressurized wells in the central area either sealed (a) or open (b).
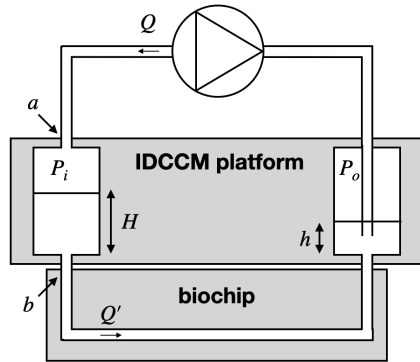
3.2 Cell growth and chip resistance

Cells tend to form a monolayer at the bottom of the biochip at low density and to assemble into multilayer structures when the number of seeded cells increases, as can be seen in supplementary figure A4. This decreases the cross-section available for the fluid in the biochip. The hydraulic resistance of empty biochips has been estimated at $5.9 \pm 0.4 \cdot 10^{12}$ kg·m^{-4}s^{-1} [22]. When cells are seeded in the biochip, this resistance increases, as illustrated in figure 3(a), where the plain line represents the fitting equation $R = 2.4 \cdot 10^7 N + 5.9 \cdot 10^{12}$ kg·m^{-4}s^{-1}. Using this correlation and taking into account the doubling time of cells, which we found was 2 days for HepG2/C3A when cultured in the chip in dynamic conditions, we can foresee the time evolution of the total number of cells and thus the time evolution of chip resistance for different seeding conditions. Figure 3(b) shows that in our biochips, the resistance varies from $R_{min} = 8.3 \cdot 10^{12}$ kg·m^{-4}s^{-1} shortly after seeding at low density (100 000 cells in the biochip) to $R_{max} = 10^{14}$ kg·m^{-4}s^{-1} after a few days of culture for cells seeded at high density (1 million per biochip). These values will be used throughout the rest of the study.

Fig. 3 Hydrodynamic resistance of a biochip seeded with cells. (a) Measurements performed for biochips seeded with variable amounts of cells. (b) Expected variation of biochip resistance over time, assuming a doubling time of 2 days, for three values of initial cell density (100 000, 500 000 and 1 000 000 cells).

3.3 Flow rate control in a tight circuit

In this section we consider a biochip connecting two wells of a culture plate installed in a IDCCM tool box as sketched in figure 4. Initially, the wells, whose cross-section area A is considered constant, are filled with culture medium up to an height h_0. The circulation of liquid from the outlet well back to the inlet well is achieved by the means of a peristaltic pump, which may lead to the displacement of air-water interfaces. H and h respectively represent the levels in the inlet and outlet wells. If the free surfaces are moving, then the flow rate Q imposed by the pump in the upper part of the circuit is not the same as the flow rate Q' inside the biochip.

Fig. 4 Experimental setup for peristaltic pump-driven circulation of fluid through a biochip. a and b respectively indicate the locations where potential leaks are considered.

If R represents the hydraulic resistance of the biochip, the pressure difference between the bottom of inlet and outlet wells is:

$$\Delta P = P_i - P_o + \rho g(H - h) = RQ' \tag{1}$$

where P_i and P_o are the pressures measured in the air above the liquid in the inlet and outlet wells. If $Q' < Q$, fluid accumulates in the inlet well:

Table 1 List and values of parameters used in the study.

Symbol	Definition	Value or range
A	Area of well cross-section	$2.01\ \text{cm}^2$
h_0	Initial position of the free surface	2 - 10 mm
H_w	Well depth	16.5 mm
R	Biochip resistance	$5 \cdot 10^{12} - 10^{14}\ \text{kg} \cdot \text{m}^{-4} \cdot \text{s}^{-1}$
Q	Flow rate imposed by the pump	10 - 25 μL/min
ρ	Density of culture medium	$1000\ \text{kg/m}^3$

$$\frac{\mathrm{d}H}{\mathrm{d}t} = \frac{Q - Q'}{A} \tag{2}$$

Since the bioreactors are placed in an incubator, the temperature is fixed. Considering air as a perfect gas we get $P_i V_i = P_{atm} V_{i_0}$, with V_i the volume of air in the inlet well. This leads to $P_i = P_{atm} \frac{H_w - h_0}{H_w - H}$, where H_w is the well depth. Similarly, $P_o = P_{atm} \frac{H_w - h_0}{H_w - h}$.

$$\Delta P = P_{atm} \left[\frac{H_w - h_0}{H_w - H} - \frac{H_w - h_0}{H_w - h} \right] + \rho g (H - h) \tag{3}$$

Mass conservation yields $H + h = 2h_0$, which makes it possible to eliminate h from (3):

$$\Delta P = P_{atm} \left(1 - \frac{h_0}{H_w} \right) \left[\frac{1}{1 - H/H_w} - \frac{1}{1 + H/H_w - 2h_0/H_w} \right] + 2\rho g (H - h_0) \tag{4}$$

Combining (2) with (4) we get

$$\frac{\mathrm{d}H}{\mathrm{d}t} = \frac{Q}{A} - \frac{P_{atm}}{AR} \left(1 - \frac{h_0}{H_w} \right) \left[\frac{1}{1 - H/H_w} - \frac{1}{1 + H/H_w - 2h_0/H_w} \right] - \frac{2\rho g}{AR} (H - h_0) \tag{5}$$

If H reaches an equilibrium value H_∞, then $\frac{\mathrm{d}H}{\mathrm{d}t} = 0$. We can then compute H_∞ by solving the 3rd-order equation:
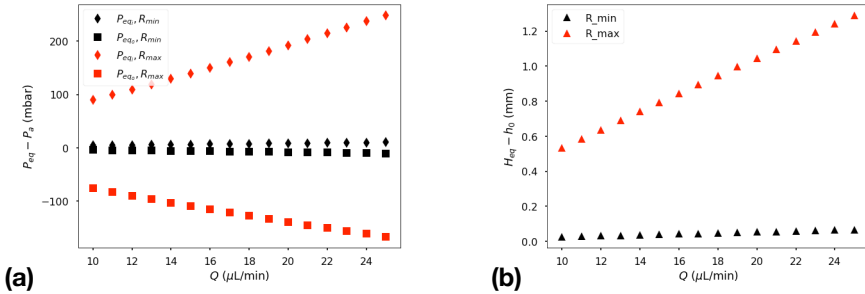
$$aH_\infty^3 + bH_\infty^2 + cH_\infty + d = 0 \tag{6}$$

with

$$\begin{cases} a & = 2\rho g \\ b & = -RQ - 6\rho g h_0 \\ c & = 2RQh_0 - 2P_{atm}(H_w - h_0) - 2\rho g(H_w^2 - 2h_0 H_w - 2h_0^2) \\ d & = RQH_w(H_w - 2h_0) + 2P_{atm}h_0(H_w - h_0) - 2\rho g h_0 H_w(2h_0 - H_w) \end{cases}$$
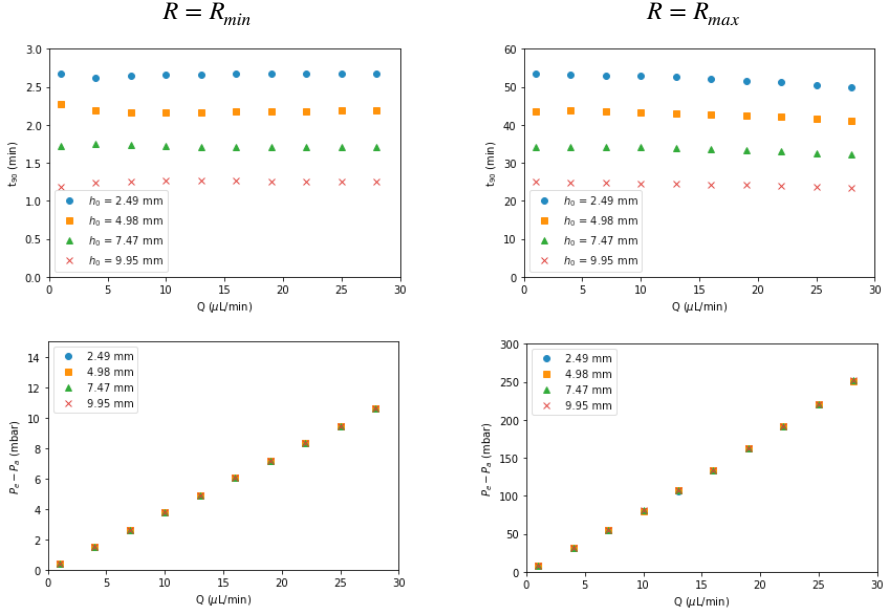
The values of a, b, c and d are computed using the numerical values of the physical parameters listed in table 1. In figure 5(**a**), pressures at equilibrium

in the inlet and outlet wells are plotted against the flow rate Q imposed by the pump. For both wells the amplitude of the relative pressure $P_{eq}-P_{atm}$ increases with Q and with R, in a more pronounced way for the inlet well. Figure 5(**b**) shows the variations of H_∞ with respect to Q for two different values of R. As long as the the biochip resistance is close to its initial value R_{min}, H_∞ remains extremely close to its initial value h_0. To increase the level of the free surface by 1 mm, the resistance needs to be much larger: $R_{max} = 10^{14}$ kg $\cdot$ m^{-4} $\cdot$ s^{-1}, which is also larger than the value measured after 3 days of culture, as seen in figure 3.

(a)   (b)

Fig. 5 Equilibrium in a tight circuit for different values of the initial fluid index h_0 in the wells. (a) Pressures in the inlet ($\diamond$) and outlet ($\square$) wells. (b) Position of the free surface in the inlet well. Red and black curves respectively indicate values obtained for $R = R_{min} = 5 \cdot 10^{12}$ kg $\cdot$ m^{-4} $\cdot$ s^{-1} and $R = R_{max} = 10^{14}$ kg $\cdot$ m^{-4} $\cdot$ s^{-1}.

$\diamond$ $\square$

For each condition, we compute the time t_{90} required for Q' to reach $90\%Q$. Figure 6 shows that Q has a limited influence on t_{90}, especially at the beginning of the experiment, when R is close to R_{min}. It is much more sensitive to variations in biochip resistance, with a quasi-linear dependency with R. The time to equilibrium also strongly depends on the amount of air initially present in the circuit. It takes more time to balance pressures in wells containing little liquid, while fuller circuits reach equilibrium sooner. When computing $P_i(t_{90})$ we notice that the pressure variations in the inlet well remain moderate as long as the biochip is not too resistive, but it can reach the tightness limit if R increases due to cell growth.

Fig. 6 Equilibrium in a tight circuit. Estimation of the time to equilibrium t_{90} and relative pressure in the inlet well as a function of Q for $R = R_{min} = 5 \cdot 10^{12}$ kg $\cdot$ m^{-4} $\cdot$ s^{-1} and $R = R_{max} = 10^{14}$ kg $\cdot$ m^{-4} $\cdot$ s^{-1}.

3.4 Influence of an air leak

As can be observed in figure 6, pressure in the inlet well reaches values at which leaks have been shown to occur in the system. In this paragraph, we therefore investigate the behavior of the free surface in the case an air leak occurs in the inlet well. We model the leak by introducing a threshold pressure P_m above which air can escape through the joint: $P_i = \min(P_m, P_{atm} \frac{H_w - h_0}{H_w - H})$. This means that the pressure drop across the biochip is smaller than the one predicted by equation (3). The leak triggers a decrease of the flow rate through the chip Q' and thus tends to amplify the accumulation of fluid in the inlet well.

As long as the system is leaking, equation (3) is replaced by

$$\Delta P = P_m - P_{atm} \frac{H_w - h_0}{H_w - h} + \rho g (H - h) \tag{7}$$
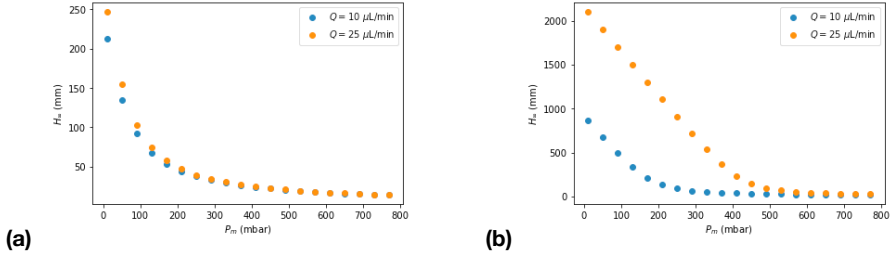
The time evolution of the system is governed by

$$\frac{dH}{dt} = \frac{Q}{A} - \frac{P_m}{AR} + \frac{P_{atm}}{AR} \frac{H_w - h_0}{H_w - 2h_0 + H} - \frac{2\rho g}{AR}(H - h_0) \tag{8}$$

This time the equilibrium height is found by solving a 2nd order equation

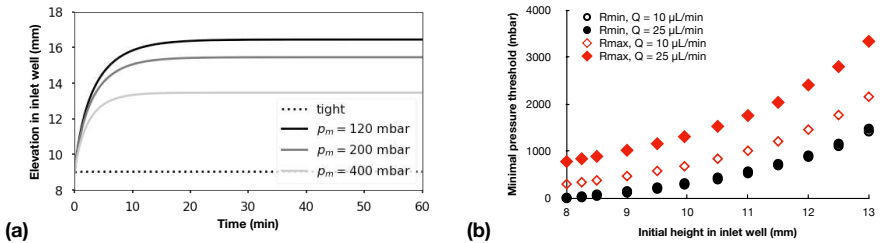$$H_\infty^2 + fH_\infty + g = 0 \tag{9}$$

with

$$\begin{cases} f &= H_w - 3h_0 + \frac{P_m - RQ}{2\rho g} \\ g &= -\frac{P_{atm}}{2\rho g}(H_w - h_0) - \left(\frac{RQ - P_m}{2\rho g} + h_0\right)(H_w - 2h_0) \end{cases}$$

Fig. 7 Equilibrium in a leaking circuit: solutions for equation (9). (a) $R = R_{min} = 5 \cdot 10^{12}$ kg $\cdot$ m^{-4} $\cdot$ s^{-1} (b) $R = R_{max} = 10^{14}$ kg $\cdot$ m^{-4} $\cdot$ s^{-1}

The resolution scheme is represented graphically in supplementary figure . In figure 7, equation (9) is solved for the extreme values of Q and R used in this study. A solution can be found but we observe that in most conditions, this solution is non-physical since the equilibrium height H_∞ is much larger than the well depth H_w. We observe that H_∞ decreases with P_m. If the circuit is sufficiently tight, an equilibrium might be reached. Figure 7 shows that in order to reach an equilibrium height $H_\infty < H_w$, the system must be able to withstand an inlet pressure of at least 507 mbar for $R = R_{max} = 10^{14}$ kg $\cdot$ m^{-4} $\cdot$ s^{-1} and $Q = 10$ μL/min, and this value increases with both R and Q. In many cases however, the level keeps growing in the inlet well.
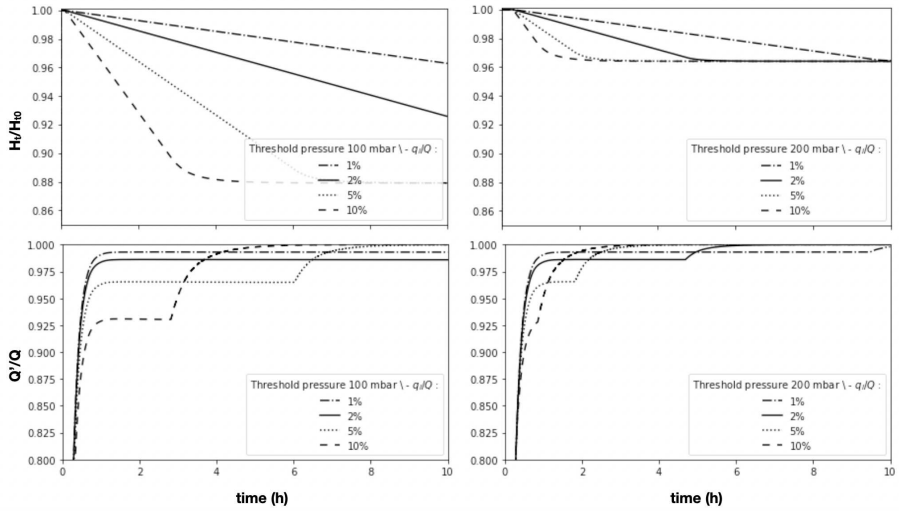

Fig. 8 Equilibrium in a leaking circuit. (a) Time evolution of the fluid index H in the inlet well for $R = R_{min}$, $h_0 = 9$ mm, $Q = 10\mu$L/min and variable value of threshold pressure p_m. (b) Variations of the minimal value of p_m compatible with an equilibrium $p_{m\,min}$ with initial position of the fluid index h_0, for extreme values of R and Q.

To determine the limit beyond which no equilibrium value is found, we proceed as sketched in figure 8 (a). We plot the time evolution of H in a tight circuit, then in a leaking circuit, starting with a large value of P_m that is progressively reduced until $H_\infty = H_w$. Figure 8 (b) shows how the pressure $P_{m_{min}}$ at which $H_\infty = H_w$ depends on the initial liquid index h in the wells.

3.5 Influence of a liquid leak

We also considered the case of a loss of liquid occurring at the inlet of the biochip due to an imperfect connector. We modeled this liquid leak as an outward flow with a constant flow rate q_l that takes place as soon as the pressure at the bottom of the inlet well reaches a limit P_l, and stops when $P_i \leq P_l$, as sketched in the diagram A3. When the circuit resistance is low $(R = R_{min})$, no leak is observed unless the threshold P_l is extremely low (5 mbar). For larger values of P_l, more compatible with experimental evaluations, the pressure drop in the biochip is so low, even for the maximal flow rate, that the inlet pressure never reaches P_l. The system keeps behaving as a tight system. On the other hand, when $R = R_{max}$, leaks occur for relevant values of P_l. The time evolution is visible in figure 9: the initially linear decrease of $H_t = H + h$ indicates that the system leaks in a constant manner at short times ; the leak then becomes intermittent in a second, transient phase ; after which finally stops and H_t reaches a plateau. The duration of each of these steps decreases with q_l, since the excess liquid is drained faster in these conditions, and with P_l. When P_l is large, the final plateau is reached sooner and the cumulated liquid loss is smaller than for small values of P_l. In all the studied cases, the flow rate Q' through the biochip is larger than 90% of the requested flow rate Q, apart from a few minutes after the pump is turned on.

Fig. 9 Effect of a leaking connector. Time evolution of the total amount of liquid in the reservoirs H_t normalized by its initial value and of the flow rate Q' through the chip normalized by the target flow rate Q, for $R = R_{max}$, $Q = Q_{max}$ and different values of the leaking flow rate q_l.

4 Conclusion

The idea to use of numerical simulations and modeling to help design microfluidic circuits and experiments is not new [23]. As microfluidic systems grow more complex, experiments involve a vast number of physical, biological and chemical parameters. One way to deal with this increasing complexity is the use of machine learning to build microfluidics databases and experimental plans but it is time- and resource- consuming[24]. In this work, we present a set of experimental data and simple simulations regarding the flow rate control in a microfluidic circuit involving free surfaces and living cells whose proliferation alter the circuit resistance.

By modeling the peristaltic pump-driven flow through a biochip installed between two wells containing a liquid-air interface, we demonstrate that, in most situations, an equilibrium state can be reached in which the flow rates through the pump and through the biochip are equal. We also found that the time to reach this equilibrium is shorter than the characteristic timescale of cell proliferation, which governs changes in hydraulic resistance. The system can thus be considered as quasi-static, with a slowly varying resistance that can be considered constant to compute the flow rate and the liquid head in both reservoirs. This result depends of course on the chosen cell line and the culture conditions. One should also keep in mind that when cells proliferate in a biochip where medium circulates at constant flow rate, they are exposed to an increasing shear stress. The target flow rate should ensure sufficient nutrient supply but prevent excessive shear stress and its value could change over the

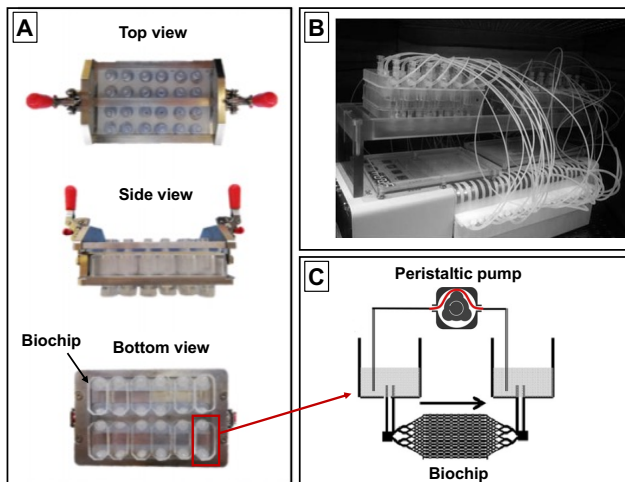course of an experiment, depending on the way the growing cells self-organize in the biochip.

We considered different leakage scenarios and demonstrated that most of them do not compromise the possibility to reach equilibrium and reach the desired flow rate. Of course, leaks have other negative consequences such as the loss of culture medium and increased risks of contamination. Making the circuit as tight as possible remains therefore an objective. We evaluated the tightness of our device at different stages of clamping force. We found that leaks occur preferentially at the wells located at the center of the device, which suggests that if an additional effort should be made to enhance tightness, these wells should be addressed first.

Our results suggest that a preliminary evaluation of cell growth, 3D organization and biochip resistance over time can be useful to design long term experiments involving recirculation and avoid leaks and contaminations, by adjusting the dimensions of biochips, volume of culture medium and degree of clamping.
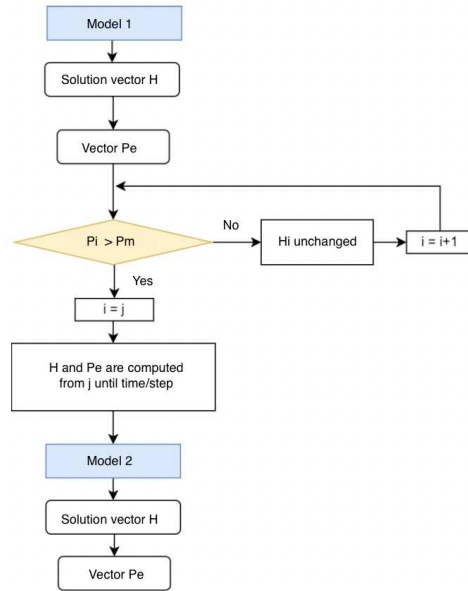
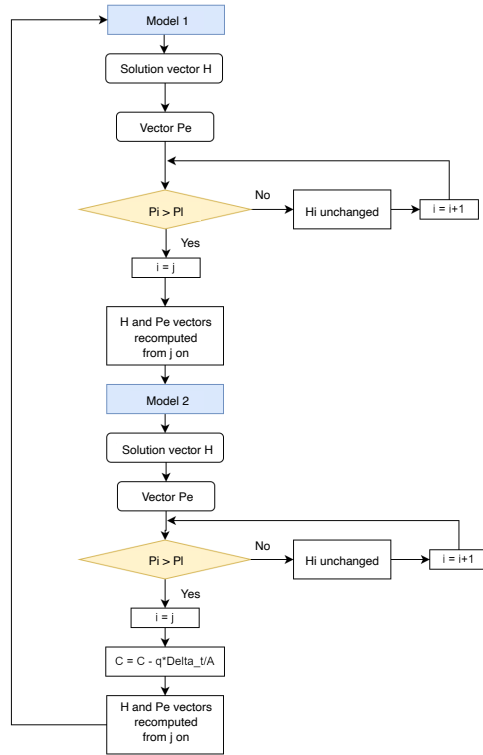**Supplementary information.**

Appendix A   Supplementary files

Fig. A1 A .Top, side and bottom views of the IDCCM platform with 12 biochips installed. B. Photograph showing the platform and connecting tuibings installed on a peristaltic pump. C. Sketch of the circuit comprising and inlet well, a biochip and an outlet well.
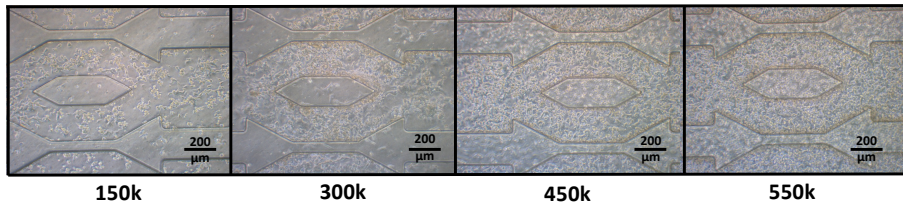
Fig. A2 Diagram illustrating the principle of resolution in the case of an air leak.

Fig. A3 Diagram illustrating the principle of resolution in the case of a liquid leak at the bottom of inlet well.

Fig. A4 Micrographs of cells in the biochip for different seeding densities.

References

[1] Byun, C.K., Abi-Samra, K., Cho, Y.-K., Takayama, S.: Pumps for microfluidic cell culture. ELECTROPHORESIS **35**(2-3), 245–257 (2013). https://doi.org/10.1002/elps.201300205

[2] Narayanamurthy, V., Jeroish, Z.E., Bhuvaneshwari, K.S., Bayat, P., Premkumar, R., Samsuri, F., Yusoff, M.M.: Advances in passively driven microfluidics and lab-on-chip devices: a comprehensive literature review and patent analysis. RSC Advances **10**(20), 11652–11680 (2020). https://doi.org/10.1039/d0ra00263a

[3] Huh, D., Bahng, J.H., Ling, Y., Wei, H.-H., Kripfgans, O.D., Fowlkes, J.B., Grotberg, J.B., Takayama, S.: Gravity-driven microfluidic particle sorting device with hydrodynamic separation amplification. Analytical Chemistry **79**(4), 1369–1376 (2007). https://doi.org/10.1021/ac061542n

[4] Jang, I., Kang, H., Song, S., Dandy, D.S., Geiss, B.J., Henry, C.S.: Flow control in a laminate capillary-driven microfluidic device. The Analyst **146**(6), 1932–1939 (2021). https://doi.org/10.1039/d0an02279a

[5] Xu, Z.-R., Yang, C.-G., Liu, C.-H., Zhou, Z., Fang, J., Wang, J.-H.: An osmotic micro-pump integrated on a microfluidic chip for perfusion cell culture. Talanta **80**(3), 1088–1093 (2010). https://doi.org/10.1016/j.talanta.2009.08.031

[6] Burger, R., Kirby, D., Glynn, M., Nwankire, C., O'Sullivan, M., Siegrist, J., Kinahan, D., Aguirre, G., Kijanka, G., Gorkin, R.A., Ducrée, J.: Centrifugal microfluidics for cell analysis. Current Opinion in Chemical Biology **16**(3-4), 409–414 (2012). https://doi.org/10.1016/j.cbpa.2012.06.002

[7] Teo, A.J.T., Li, K.-H.H., Nguyen, N.-T., Guo, W., Heere, N., Xi, H.-D., Tsao, C.-W., Li, W., Tan, S.H.: Negative pressure induced droplet generation in a microfluidic flow-focusing device. Analytical Chemistry **89**(8), 4387–4391 (2017). https://doi.org/10.1021/acs.analchem.6b05053

[8] Li, Z., Mak, S.Y., Sauret, A., Shum, H.C.: Syringe-pump-induced fluctuation in all-aqueous microfluidic system implications for flow rate accuracy. Lab on a Chip **14**, 744 (2014)

[9] Zeng, W., Jacobi, I., Li, S., Stone, H.A.: Variation in polydispersity in pump- and pressure-driven micro-droplet generators. Journal of Micromechanics and Microengineering **25**(11), 115015 (2015). https://doi.org/10.1088/0960-1317/25/11/115015

[10] Ward, T., Faivre, M., Abkarian, M., Stone, H.A.: Microfluidic flow focusing: Drop size and scaling in pressure versus flow-rate-driven pumping. Electrophoresis **26**, 3716–3724 (2005)

[11] Bihi, I., Vesperini, D., Kaoui, B., Le Goff, A.: Pressure-driven flow focusing of two miscible liquids. Physics of Fluids **31**(6), 062001 (2019). https://doi.org/10.1063/1.5099897

[12] Oh, K.W., Lee, K., Ahna, B., Furlani, E.P.: Design of pressure-driven microfluidic networks using electric circuit analogy. Lab on a Chip **12**, 515–545 (2012)

[13] Minetti, F., Giorello, A., Olivares, M.L., Berli, C.L.A.: Exact solution of the hydrodynamic focusing driven by hydrostatic pressure. Microfluidics and Nanofluidics **24**(2) (2020). https://doi.org/10.1007/s10404-020-2322-y

[14] Bong, K.W., Chapin, S.C., Pregibon, D.C., Baah, D., Floyd-Smith, T.M., Doyle, P.S.: Compressed-air flow control system. Lab Chip **11**(4), 743–747 (2011). https://doi.org/10.1039/c0lc00303d

[15] Mavrogiannis, N., Ibo, M., Fu, X., Crivellari, F., Gagnon, Z.: Microfluidics made easy: A robust low-cost constant pressure flow controller for engineers and cell biologists. Biomicrofluidics **10**(3), 034107 (2016). https://doi.org/10.1063/1.4950753

[16] Gnyawali, V., Saremi, M., Kolios, M.C., Tsai, S.S.H.: Stable microfluidic flow focusing using hydrostatics. Biomicrofluidics **11**(3), 034104 (2017). https://doi.org/10.1063/1.4983147

[17] de Graaf, M.N.S., Vivas, A., van der Meer, A.D., Mummery, C.L., Orlova, V.V.: Pressure-driven perfusion system to control, multiplex and recirculate cell culture medium for organs-on-chips. Micromachines **13**(8), 1359 (2022). https://doi.org/10.3390/mi13081359

[18] Futai, N., Gu, W., Song, J.W., Takayama, S.: Handheld recirculation system and customized media for microfluidic cell culture. Lab Chip **6**(1), 149–154 (2006). https://doi.org/10.1039/b510901a

[19] Garcia-Cordero, J.L., Basabe-Desmonts, L., Ducrée, J., Ricco, A.J.: Liquid recirculation in microfluidic channels by the interplay of capillary and centrifugal forces. Microfluidics and Nanofluidics **9**(4-5), 695–703 (2010). https://doi.org/10.1007/s10404-010-0585-4

[20] Debski, P., Sklodowska, K., Michalski, J., Korczyk, P., Dolata, M., Jakiela, S.: Continuous recirculation of microdroplets in a closed loop tailored for screening of bacteria cultures. Micromachines **9**(9), 469 (2018). https://doi.org/10.3390/mi9090469

[21] Baudoin, R., Alberto, G., Paullier, P., Legallais, C., Leclerc, E.: Parallelized microfluidic biochips in multi well plate applied to liver tissue engineering. Sensors and Actuators B: Chemical **173**, 919–926 (2012). https://doi.org/10.1016/j.snb.2012.06.050

[22] Messelmani, T., Le Goff, A., Souguir, Z., Maes, V., Roudaut, M., Vandenhaute, E., Maubon, N., Legallais, C., Leclerc, E., Jellali, R.: Development of liver-on-chip integrating a hydroscaffold mimicking the liver's extracellular matrix. Bioengineering **9**(9), 443 (2022). https://doi.org/10.3390/bioengineering9090443

[23] Erickson, D.: Towards numerical prototyping of labs-on-chip: modeling for integrated microfluidic devices. Microfluidics and Nanofluidics **1**(4), 301–318 (2005). https://doi.org/10.1007/s10404-005-0041-z

[24] McIntyre, D., Lashkaripour, A., Fordyce, P., Densmore, D.: Machine learning for microfluidic design and control. Lab on a Chip **22**(16), 2925–2937 (2022). https://doi.org/10.1039/d2lc00254j